# REPORT DOCUMENTATION PAGE

*Form Approved*
*OMB No. 0704-0188*



| 1. REPORT DATE *(DD-MM-YYYY)* | 2. REPORT TYPE | 3. DATES COVERED *(From - To)* |
|---|---|---|
| | New Reprint | |

**4. TITLE AND SUBTITLE**
Graphene Sheets Stabilized on Genetically Engineered M13 Viral Templates as Conducting Frameworks for Hybrid Energy-Storage Materials

**5a. CONTRACT NUMBER**

**5b. GRANT NUMBER**
W911NF-09-D-0001

**5c. PROGRAM ELEMENT NUMBER**
611104

**6. AUTHOR(S)**
Dahyun Oh, Xiangnan Dang, Hyunjung Yi, Mark A. Allen, Kang Xu, Yun Jung Lee, Angela M. Belcher

**5d. PROJECT NUMBER**

**5e. TASK NUMBER**

**5f. WORK UNIT NUMBER**

**7. PERFORMING ORGANIZATION NAME(S) AND ADDRESS(ES)**
University of California - Santa Barbara
Office of Research
The Regents of the University of California
Santa Barbara, CA 93106 -2050

**8. PERFORMING ORGANIZATION REPORT NUMBER**

**9. SPONSORING/MONITORING AGENCY NAME(S) AND ADDRESS(ES)**
U.S. Army Research Office
P.O. Box 12211
Research Triangle Park, NC 27709-2211

**10. SPONSOR/MONITOR'S ACRONYM(S)**
ARO

**11. SPONSOR/MONITOR'S REPORT NUMBER(S)**
55012-LS-ICB.422

**12. DISTRIBUTION/AVAILABILITY STATEMENT**
Available for public release; distribution unlimited

**13. SUPPLEMENTARY NOTES**
The views, opinions and/or findings contained in this report are those of the author(s) and should not construed as an official Department of the Army position, policy or decision, unless so designated by other documentation.

**14. ABSTRACT**
See attached.

**15. SUBJECT TERMS**
None.

| 16. SECURITY CLASSIFICATION OF: | | | 17. LIMITATION OF ABSTRACT | 18. NUMBER OF PAGES | 19a. NAME OF RESPONSIBLE PERSON |
|---|---|---|---|---|---|
| a. REPORT | b. ABSTRACT | c. THIS PAGE | | | Francis Doyle |
| | | | | | 19b. TELEPHONE NUMBER *(Include area code)* |
| UU | UU | UU | UU | | 805-893-8133 |

## REPORT DOCUMENTATION PAGE (SF298)
## (Continuation Sheet)

Continuation for Block 13

ARO Report Number 55012.422-LS-ICB
Graphene Sheets Stabilized on Genetically Eng...

Block 13: Supplementary Note

## Report Title

Graphene Sheets Stabilized on Genetically Engineered M13 Viral Templates as Conducting Frameworks for Hybrid Energy-Storage Materials

## ABSTRACT

See attached.

# Graphene Sheets Stabilized on Genetically Engineered M13 Viral Templates as Conducting Frameworks for Hybrid Energy-Storage Materials

*Dahyun Oh, Xiangnan Dang, Hyunjung Yi, Mark A. Allen, Kang Xu, Yun Jung Lee,* and Angela M. Belcher**

Single-layer graphene sheets have significantly broadened the horizon of nanotechnology with the unique electronic, optical, quantum mechanical and mechanical properties associated with the two-dimensional atomic crystal structure.[1] To best utilize this material for practical applications, it is crucial to prevent the spontaneous aggregation between individual graphene sheets while composite materials are formed. Numerous efforts have been made to stabilize functionalized graphene sheets on molecular[2] or polymeric species.[3,4] Biomolecules such as DNA[5] and proteins[6] have also been grafted onto graphene planes and used for biosensors,[7] controlled drug-delivery[8] as well as cancer imaging.[9] As well as biomedical applications, graphene sheets can also be hybridized with biomolecules into energy-storage devices to increase the conductivity of the active materials that are often insulators. In previous work, ultrasonication[10] or chemical reduction,[11] followed by heat treatment,[12–14] have been adopted to achieve composites between graphene and various materials (e.g., $LiFePO_4$[10] and $SnO_2$[15]). However, due to the non-specific nature of the interactions between the graphene templates and active materials, it is expected that only random and inhomogeneous contacts are created, leaving the segregation on nano- or even sub-micrometer levels. Ideally, the performance of these active materials, such as the accessible capacity and the rate capability, can be maximized only if atomic level contacts can be realized between the conductive phase (graphene) and the active phase.

In order to expand the range of graphene-based hybrid materials, methods to prevent aggregation around the limit of colloidal stability need to be developed. The stability of aqueous colloidal dispersion of functionalized graphene is usually maintained at high pH and low ionic strength due to the charges on the functionalized surface.[16] Substrate specificity of ligands in biomolecules can improve the colloidal stability of graphene and strengthen the interaction between graphene and functional materials, thereby providing a genetically tunable hybrid building block and a desired conducting frame. The M13 bacteriophage has been demonstrated as a genetically engineerable biological toolkit to develop nanostructured hybrid materials to enhance the performance of energy-storage and -conversion devices.[17,18] Here, we show that the noncovalent binding between the engineered M13 virus and graphene increased the dispersion stability of graphene sheets at a pH as low as 3 and an increased ionic strength environment. In addition, using this biological engineering approach, we were able to take a DNA sequence that coded for peptides and that could bind graphene, and modified this sequence to further broaden the stability window of the aqueous colloid of graphene sheets. With the improved stability of graphene in aqueous media, inorganic nanoparticles nucleated on the M13 virus were able to intimately interface with graphene sheets and fully utilized the excellent electronic conductivity of graphene, although the incorporation of graphene might lower the packing density. As a result, we achieved an efficient conducting matrix throughout the hybrid material with the genetically engineered M13 virus, which simultaneously stabilizes graphene sheets and mineralizes the active nanoparticles. We also demonstrated that the electrochemical utilization of the originally insulating active materials could be maximized in the composite network consisting of active nanoparticles and conductive graphene sheets.

We utilized an M13 virus to synthesize a graphene/virus complex to function as a building block for a conducting framework. The M13 virus is a filamentous bacteriophage,

D. Oh, X. Dang, H. Yi, Dr. M. A. Allen, Prof. A. M. Belcher
Department of Materials Science and Engineering
The David H. Koch Institute for Integrative Cancer Research
Massachusetts Institute of Technology
Cambridge, Massachusetts 02139, USA
E-mail: belcher@mit.edu
Dr. K. Xu
Electrochemistry Branch
Power & Energy Division
Sensor and Electron Devices Directorate U. S. Army
Research Laboratory
Adelphi, Maryland, 20783, USA
Prof. Y. J. Lee
Department of Energy Engineering
Hanyang University
Seoul 133-791, Republic of Korea
E-mail: yjlee94@hanyang.ac.kr
Prof. A. M. Belcher
Department of Biological Engineering
Massachusetts Institute of Technology
Cambridge, Massachusetts 02139, USA

DOI: 10.1002/smll.201102036

small NANO MICRO

with a length of ~880 nm and a diameter of ~6.5 nm.[19] The single-stranded DNA encapsulated inside the coat proteins can be modified to express specific peptide sequences on the surface of the virus to enhance the interaction with materials of interest.[20,21] To fabricate a virus-mediated graphene framework with inorganic nanoparticles, two factors must be addressed: the colloidal stability of graphene, and the interface between the active materials and the graphene. In designing an M13 virus, the major coat protein (pVIII) was chosen as a major interacting motif to maximize the attraction between the graphene and the virus, so that every particle templated on the virus was forced to contact the graphene (**Figure 1**a). First, the graphene-binding virus, with an 8-mer peptide insert (DVYESALP) fused to the amino-terminus of the pVIII major coat protein (this virus is called p8cs#3), was identified through a bio-panning method using a pVIII library previously reported by this group.[18] The aromatic residue, tyrosine (Y), of the selected sequence is expected to interact with graphene, as well as single-walled carbon nanotubes (SWNTs), through $\pi$–$\pi$ interactions. In addition to the aromatic residue, the hydrophobicity plot of the sequence, calculated based on the Hopp–Woods scale with the averaging group size five,[22] shows a hydrophobic moiety between two hydrophilic regions (Figure 1b inset) suggesting that the virus can bind graphene by hydrophobic–hydrophobic interaction. Second, to facilitate the nucleation of nanoparticles, we introduced two additional carboxyl groups on each pVIII protein of p8cs#3 virus, in which the thirteenth amino acid, lysine (K), and the seventeenth amino acid, asparagine (N), were changed to the glutamic acid (E), using site-directed mutagenesis (Figure 1b top) (this site-mutated virus is called EFE). Since the thirteenth and seventeenth amino acids of an M13 virus are known to be exposed on the surface and accessible to ligands,[23] these carboxyl groups of glutamic acid can chelate metal ions and catalyze the mineralization. The zeta potential of EFE was measured and compared

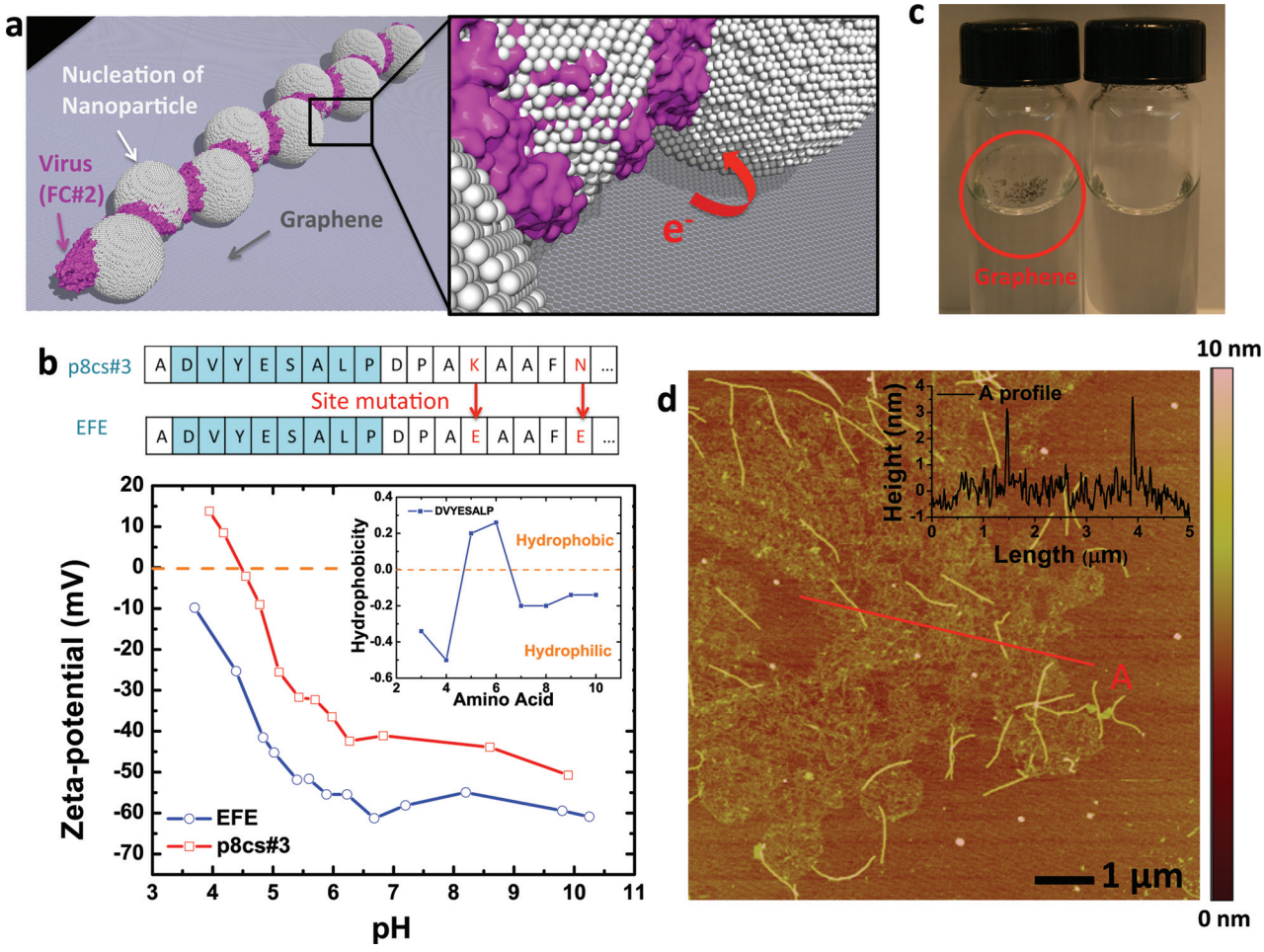


**Figure 1.** The graphene/virus complex with the enhanced colloidal stability of the hybrid graphene/nanoparticle nanocomposites. a) Scheme of the inorganic-nanoparticle nucleation on the graphene/virus template. The virus enables a close contact between inorganic nanoparticles and the graphene. b) Top: The peptide sequence of pVIII protein of p8cs#3 and EFE. Bottom: The zeta potential of EFE and p8cs#3. Inset: The hydrophobicity plot of the pVIII major coat proteins of p8cs#3 virus as a function of the amino acid location. c) The left vial is the graphene solution after 24 h incubation with bismuth nitrate, showing the aggregation of graphene on top. The right vial is the graphene/FC#2 complex solution after 24 h incubation with bismuth nitrate without any aggregation. d) AFM image of the graphene/FC#2 complex. Inset: The height profile of line A showing the thickness of graphene as ~0.8 nm.

with that of the control virus, p8cs#3, to confirm the effect of the site-directed mutation on the surface charge of the virus (Figure 1b bottom). It was observed that the isoelectric point of the virus shifted to a lower pH by the addition of two glutamic acids on the pVIII protein. The increased negative charges associated with the carboxyl groups have additional advantages in enhancing the colloidal stability of the graphene/virus complex. Finally, the pIII minor coat protein was also engineered to increase the binding affinity between the virus and the graphene (see the method in the Supporting Information (SI)). We designate this virus clone as FC#2 and use it for further research on stabilizing graphene, nucleating functional materials, and improving the performance of lithium-ion batteries. The stability of the graphene/virus complex was tested by adding bismuth nitrate (the precursor of the material of interest for lithium-ion batteries) at pH 3. The stability of graphene dispersion by the virus was maintained after 24 h incubation with bismuth nitrate as shown in Figure 1c. This is in contrast to the control sample under the same salt concentration and pH without the virus, where the graphene aggregated. We also observed the graphene/FC#2 complex by atomic force microscopy (AFM) (Figure 1d). An area with lower coverage of the virus on the graphene, compared with the approximate calculation (see SI for the calculation), was selected to clearly visualize the interaction of the virus and the graphene. The thickness of the graphene in the solution was around 0.8 nm as indicated in the Figure 1d inset.

Utilizing the enhanced colloidal stability of the genetically programmed graphene/virus complex, we assembled bismuth oxyfluoride on the graphene/virus template. Bismuth oxyfluoride is a conversion-reaction cathode material with an open-circuit voltage of 2.8 V vs $Li/Li^+$, a high theoretical specific capacity of 210 mAh $g^{-1}$ (for $BiO_{0.5}F_2$, from LiF formation) and an attractive volumetric energy density of 5056 Wh $L^{-1}$ (for $BiO_{0.5}F_2$, higher than $LiCoO_2$ with 2845 Wh $L^{-1}$),[24] which can be synthesized in aqueous solution under low pH conditions. Among the candidates of cathode materials for next-generation lithium-ion batteries, bismuth oxyfluoride was chosen as a model material, since we found the synthetic condition for this material under a weakly acidic environment, suitable for demonstrating the improved colloidal stability of the graphene. Since the M13 virus helped maintain the colloidal stability of the graphene during the nucleation of inorganic nanoparticles under low pH, it is now possible to form hybrid nanostructures of the graphene/(bismuth oxyfluoride). We first developed an aqueous solution-based approach to synthesize bismuth oxyfluoride nanoparticles on the virus under a weakly acidic condition at room temperature, using LiF as a milder precursor than hydrofluoric acid[25] and ammonium fluoride.[26] Nanoparticles, thus synthesized, have a diameter of around 40 nm (**Figure 2**a,b). The virus-mediated synthesis increased the reaction yield (from 17% without virus, to 63% with virus, both without graphene) and decreased the particle-size of the material compared with the previous report.[25] To fabricate the nanocomposites of the water-soluble graphene (Figure 2c) and bismuth oxyfluoride, the graphene was first complexed and stabilized by the FC#2 virus, and then bismuth oxyfluoride was grown on the graphene/virus complex. In order to visualize the hybrid structure with graphene, we used a lowered concentration of the precursor to show that more bismuth oxyfluoride was nucleated along the virus than on the surface of graphene (Figure 2d). The chemically modified graphene (see SI for graphene synthesis) possesses functional groups, which also act as nucleation sites, but the graphene-assisted nucleation is not as efficient as the virus-assisted nucleation. Two control hybrid materials with the graphene were synthesized without using the virus, or with a wild-type virus (M13KE, denoted in our work as a wild-type virus). In addition to the reduced colloidal stability as shown in Figure 1c, the yield of bismuth oxyfluoride from the reaction without the virus (42%) was much lower than the yield from the reaction aided by the FC#2 (68%). For the nanocomposites made with the wild-type virus the graphene was initially stabilized by non-specific interaction, but the graphene aggregation, and the separation between the graphene and active materials, eventually prevailed as the nucleation proceeded (Figure 2e). Furthermore, the positive surface-charge from the wild-type virus under weakly acidic conditions (pH 3) did not facilitate the nucleation of bismuth oxyfluoride and the yield was similar to the reaction without the virus.

The crystal structure of the virus-templated bismuth oxyfluoride was confirmed as cubic $Fm\bar{3}m$ by HRTEM (Figure 2b) and X-ray diffraction (XRD) (Figure 2f), with a lattice parameter of 5.8160(1) Å. From X-ray photoelectron spectroscopy (XPS) elemental analysis, the bismuth-to-fluorine ratio was determined to be 1:2.02 (see Table S2 of the SI), giving a chemical formula of $BiO_{0.49}F_{2.02}$. The galvanostatic measurement (at a current density of 6 mA $g^{-1}$) further confirmed the composition of fluorine and oxygen based on the fact that oxygen and fluorine in bismuth oxyfluoride react with the lithium at different potentials of 1.8 and 2.6 V vs $Li/Li^+$.[24] In Figure S2B of the SI, the ratio of discharge capacity in the plateau regions around 2.7 V and 1.9 V was calculated to be 1.95:1.05. Because the ethyl methyl carbonate (EMC) electrolyte is inert to Bi nanocrystals,[27] the solid electrolyte interphase formation does not occur under 2 V; therefore, does not contribute to the capacity. Since each fluorine atom reacts with one lithium atom and each oxygen atom reacts with two lithium atoms, the galvanostatic measurement gave a chemical formula of $BiO_{0.525}F_{1.95}$, in fairly good agreement with the XPS analysis result. Therefore, we concluded with a reasonable approximation that the chemical formula of the synthesized bismuth oxyfluoride was close to $BiO_{0.5}F_2$.

The advantage of incorporating well-dispersed graphene into lithium-ion battery cathodes was demonstrated by making electrodes with the graphene/(bismuth oxyfluoride) nanocomposites assembled with a biologically engineered virus. With a small amount (2.4 wt%) of graphene incorporated into the bismuth oxyfluoride, the specific capacity of the virus-templated bismuth oxyfluoride was increased from 124 mAh $g^{-1}$ to 174 mAh $g^{-1}$ at a current density of 30 mA $g^{-1}$ (C/7) (**Figure 3**a,b). The second-cycle capacity (206 mAh $g^{-1}$, at C/7) of the virus-templated bismuth oxyfluoride with 2.4 wt% of graphene (in Figure S4 of the SI) corresponds to 98% of theoretical capacity, which is the highest reported for this material to date. Moreover, the rate performance has also

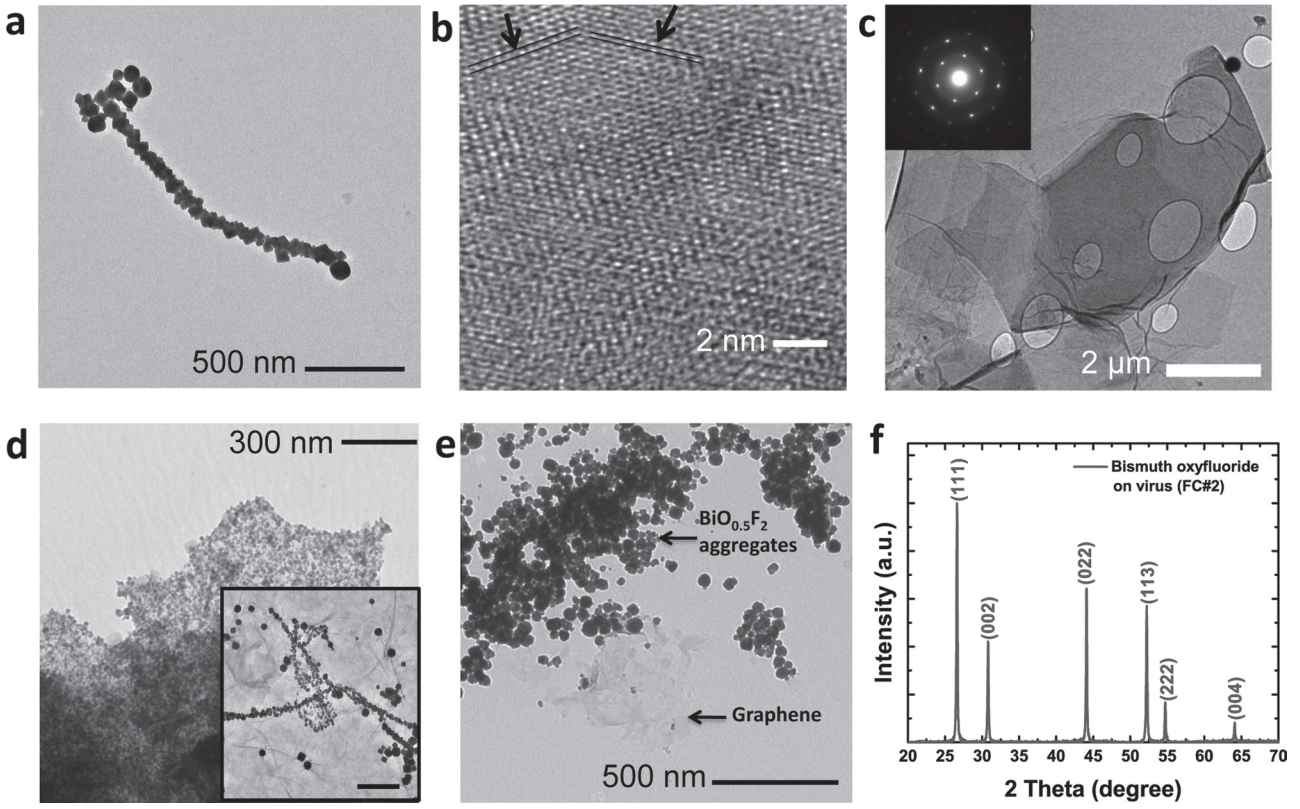


**Figure 2.** Characterizations of the bismuth oxyfluoride nucleated on the graphene/virus complex. a) TEM image of bismuth oxyfluoride nucleated on FC#2. b) High-resolution transmission electron microscopy (HRTEM) image of a bismuth oxyfluoride nanoparticle with the $Fm\bar{3}m$ crystal system, (200) $d$ (the distance between adjacent atomic planes) = 2.9 Å (left arrow), and (220) $d$ = 2.1 Å (right arrow). c) TEM image of the chemically reduced graphene with a selected-area electron diffraction (SAED) pattern. d) TEM image of the (bismuth oxyfluoride)/graphene nanocomposites with FC#2 virus for battery electrodes. The (bismuth oxyfluoride)/FC#2 virus complexes are shown exclusively on the graphene. Inset: Catalyzed nucleation of bismuth oxyfluoride on FC#2 virus was observed by lowering the precursor concentration in the composite synthesis. The background of the inset is graphene and a scale bar of 400 nm is shown. e) TEM image of the (bismuth oxyfluoride)/graphene nanocomposites formed with the wild-type virus showing the separation of graphene and bismuth oxyfluoride. f) X-ray diffraction (XRD) pattern of bismuth oxyfluoride nanoparticles.

been improved, showing a specific capacity of 131 mAh $g^{-1}$ (corresponding to 711 W $kg^{-1}$, with an energy density of 316 Wh $kg^{-1}$, 2718 Wh $L^{-1}$) at a current density of 300 mA $g^{-1}$ (1.4 C) compared with a specific capacity of 67 mAh $g^{-1}$ (at 1.4 C) for the virus-templated bismuth oxyfluoride without graphene. These results represent a significant improvement in the electrochemical performance of bismuth oxyfluoride compared with the previous report, as indicated by the increased active-mass loading in the electrode (from 50 wt% to 70 wt%) and the improved specific capacity at a 20-times-higher current density. In addition, the presence of the graphene also significantly decreased the voltage hysteresis between the charge and the discharge profiles (Figure S4 of the SI), which became more pronounced at a higher discharging rate (Figure 3a). This reduction in the electrode overpotential stems from the excellent electrical wiring achieved at the atomic level by graphene sheets, which connects active nanoparticles with the cell-current collector through a homogeneously distributed percolating conductive network.

To study the beneficial effect of specific interaction between the genetically engineered virus and the graphene in the formation of a conducting framework, control experiments have been done with graphene/(bismuth oxyfluoride) nanocomposites synthesized in the absence of the virus or in the presence of the wild-type virus. The bismuth oxyfluoride synthesized in the control experiments had the same chemical and crystallographic properties as that formed with FC#2 (Figure S5 in the SI shows XRD patterns for each composite). As shown in Figure 3a–d, the specific capacity (174 mAh $g^{-1}$ at C/7) of nanocomposites using FC#2 was higher than that of nanocomposites using the wild-type virus (145 mAh $g^{-1}$ at C/7) and without the virus (102 mAh $g^{-1}$ at C/7). Moreover, the superior electrochemical performance of the nanocomposites using FC#2 was more apparent at a high rate of 600 mA $g^{-1}$ (110 mAh $g^{-1}$ for FC#2, 67 mAh $g^{-1}$ for the wild-type virus, and 64 mAh $g^{-1}$ without the virus), indicating accelerated electrode kinetics for the cell reactions in those nanocomposites benefiting from the specific interaction between the graphene and FC#2 virus. The poor electrochemical activities of the nanocomposites in the presence of the wild-type virus and in the absence of the virus, are caused by the agglomeration of graphene during the active material synthesis. Based on these observations, we conclude that the increased interaction of graphene with the active material particles aided by the genetically engineered virus results in an efficient conducting network. This was made possible by

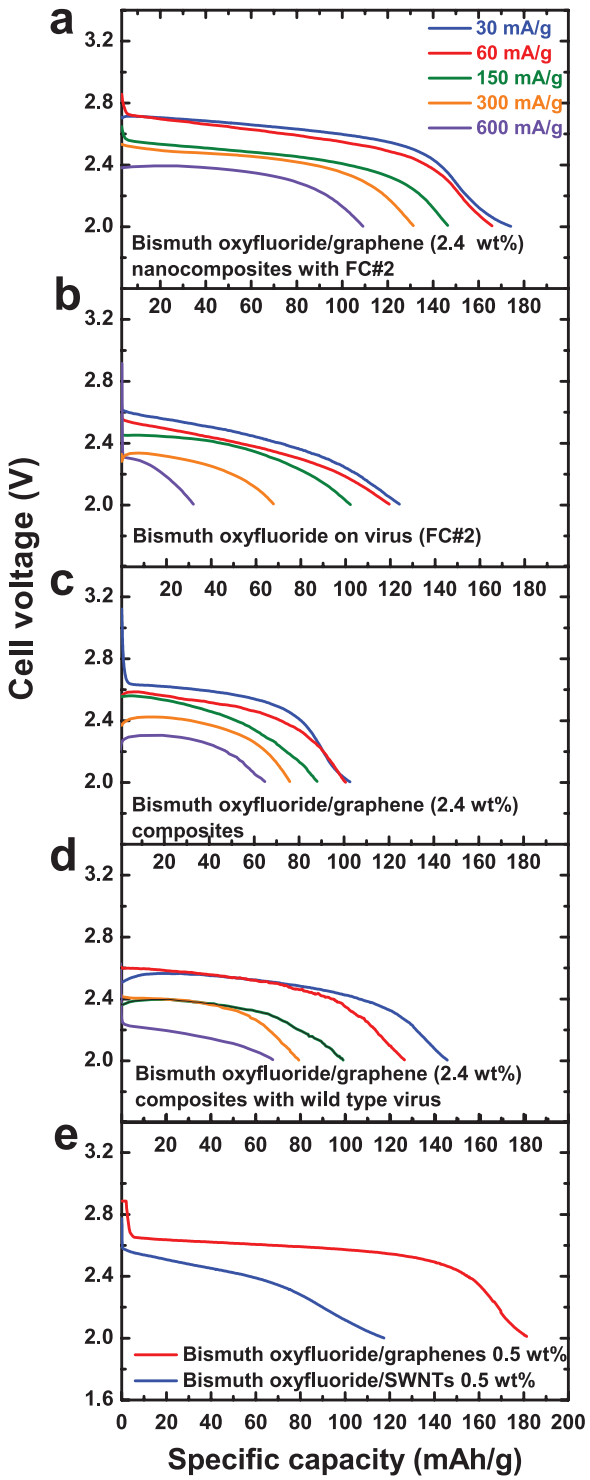


**Figure 3.** The power performance of the graphene/(bismuth oxyfluoride) nanocomposites with the genetically engineered M13 virus. a–d) The first discharge of bismuth oxyfluoride at different current densities: a) the (bismuth oxyfluoride)/graphene nanocomposites with FC#2; b) the bismuth oxyfluoride templated on FC#2 without graphene; c) the (bismuth oxyfluoride)/graphene composites in the absence of virus; and d) the (bismuth oxyfluoride)/graphene composites in the presence of the wild-type virus. e) Comparison between the first discharge of the (bismuth oxyfluoride)/graphene composites and the (bismuth oxyfluoride)/SWNTs composites formed with FC#2 viruses, having the same mass percentage of carbon (0.5 wt% of electrodes) at 30 mA $g^{-1}$ current density.

maintaining the colloidal stability of complex during the synthesis. Moreover, we achieved both higher capacity utilization of the active materials and a much reduced kinetic barrier between charge and discharge reactions, as compared with the previous report.[24]

The superior formation of a percolating network with two-dimensional conducting sheets, enabled by the genetically engineered virus, has also been demonstrated by comparing the effects of graphene and SWNTs on the electrochemical performance of bismuth oxyfluoride. The SWNTs were evenly dispersed inside the electrode by the virus complexation method[18] and bismuth oxyfluoride was synthesized on this template. When the same amount of graphene and SWNTs (0.5 wt%) were incorporated into the nanocomposites, the specific capacities of 128 mAh $g^{-1}$ for the SWNTs/(bismuth oxyfluoride) nanocomposites and 181 mAh $g^{-1}$ for the graphene/(bismuth oxyfluoride) nanocomposites were obtained respectively, at a current density of 30 mA $g^{-1}$ (Figure 3e). The graphene improves the kinetics of the conversion reaction more effectively than SWNTs. Although the SWNTs are known to be advantageous for constructing a percolating network because of their high aspect ratio,[28] when a small quantity of carbon is used, the interconnectivity between the one-dimensional SWNTs could be limited compared with the two-dimensional graphene. In the bismuth oxyfluoride system, the graphene appears to be more effective in facilitating the electrochemical reaction.

In summary, using a genetically engineered M13 virus, we broadened the stability window of graphene in aqueous media, which enabled an environmentally friendly approach to establish a graphene/virus nanotemplate. By designing the M13 virus for simultaneously stabilizing the graphene and nucleating bismuth oxyfluoride, we fabricated the graphene/(bismuth oxyfluoride) nanocomposites in which both phases were intimately interwoven. The graphene/virus complex formed a homogeneously distributed conducting framework and the kinetics of electron transfer inside the battery electrodes was improved, demonstrating the increased specific capacity of bismuth oxyfluoride at a high current density (131 mAh $g^{-1}$ at 300 mA $g^{-1}$) and the reduced overpotentials for both charging and discharging cell reactions. This study demonstrates the importance of well-dispersed graphene in aqueous media for synthesizing composite materials and this general method could be extended to other materials for applications including biosensors, supercapacitors, catalysts and energy-conversion applications.

## Experimental Section

*Synthesis of Bismuth Oxyfluoride Powders, Bismuth Oxyfluoride and Graphene Nanocomposites for FC#2 Virus, Wild-type Virus, and without Virus*: FC#2 viruses ($2 \times 10^{13}$) were incubated with the graphene solution (64 mL, 2.3 μg $mL^{-1}$). $Bi(NO_3)_3 \cdot 5H_2O$ (0.8 mL, 200 mM, dissolved in 10% $HNO_3$) was added to this mixture to make the final solution (400 mL, 0.4 mM). LiF solution (171 mL, 50 mM) was added and stirred at room temperature for 3 h. Graphene solution (40 mL, 50 μg $mL^{-1}$) was further added into the nanocomposites. The final products were filtered, washed and

small NANO MICRO

dried under vacuum at 50 °C overnight. With the same method, wild-type viruses were used for (bismuth oxyfluoride)/graphene nanocomposites and virus addition and incubation steps were excluded for composites without virus.

*Synthesis of Bismuth Oxyfluoride and SWNTs Nanocomposites*: The SWNT/FC#2 complexes were constructed by dialyzing the mixture of FC#2 ($2 \times 10^{13}$) and SWNTs (0.094 mg in 2 wt% sodium cholate aqueous solution) against deionized water with gradual increase of salt (KCl) concentration of media from 10 mM to 80 mM, while maintaining pH 9 using NaOH for two days. Bismuth oxyfluoride was synthesized by adding $Bi(NO_3)_3 \cdot 5H_2O$ (0.8 mL, 200 mM, dissolved in 10% $HNO_3$) to the complex solution giving a final volume of 400 mL. After an hour, LiF (171 mL, 50 mM) was added and the solution was left to stand for 2 h. The final products were washed and dried under vacuum at 50 °C overnight.

*Electrochemical Tests*: Active materials were mixed mechanically with carbon black (SUPER P® Li, TIMCAL) for 20 min and polytetrafluoroethylene (PTFE) was added. The mass ratio of (active materials):virus:graphene:(carbon black):PTFE was 68.8: 8.8: 2.4: 15: 5. Mixed powders were rolled out and punched, in 4.08 mg $cm^{-2}$ quantities, then dried under vacuum at 120 °C overnight. Inside the Ar-filled glove box, the electrodes were assembled into coin cells with Li-metal foils as the counter electrodes and 1 M $LiPF_6$ in EMC was used as the electrolyte. Three layers of microporous polymer separator (Celgard 2325) were used. Assembled coin cells were tested with a Solatron Analytical 1470E potentiostat at room temperature.

## Supporting Information

*Supporting Information is available from the Wiley Online Library or from the author.*

## Acknowledgements

*This work was supported by the Army Research Office Institute through the Institute of Collaborative Biotechnologies (ICB) and US National Science Foundation through the Materials Research Science and Engineering Centers program. The authors appreciate the discussions with Prof. Gerbrand Ceder; the assistance in dispersing SWNT from Prof. Moon-Ho Ham; the XRD analysis by Dr. Scott A. Speakman; and discussions with Prof. Byungwoo Kang. DO is grateful for Kwanjeong Educational Foundation Scholarship and HY is grateful for a Korean Government Overseas Scholarship.*

[1] A. K. Geim, K. S. Novoselov, *Nat. Mater.* **2007**, *6*, 183.
[2] D. Petridis, A. B. Bourlinos, D. Gournis, T. Szabo, A. Szeri, I. Dekany, *Langmuir* **2003**, *19*, 6050.
[3] H. J. Salavagione, M. A. Gomez, G. Martinez, *Macromolecules* **2009**, *42*, 6331.
[4] G. Q. Shi, H. Bai, Y. X. Xu, L. Zhao, C. Li, *Chem. Commun.* **2009**, 1667.
[5] V. Berry, N. Mohanty, *Nano Lett.* **2008**, *8*, 4469.
[6] M. X. Ye, J. F. Shen, M. Shi, B. Yan, H. W. Ma, N. Li, Y. Z. Hu, *Colloid Surf. B* **2010**, *81*, 434.
[7] J. H. Jiang, Q. Zeng, J. S. Cheng, X. F. Liu, H. T. Bai, *Biosens. Bioelectron.* **2011**, *26*, 3456.
[8] Z. Liu, J. T. Robinson, X. Sun, H. Dai, *J. Am. Chem. Soc.* **2008**, *130*, 10876.
[9] X. Sun, Z. Liu, K. Welsher, J. T. Robinson, A. Goodwin, S. Zaric, H. Dai, *Nano Res.* **2008**, *1*, 203.
[10] X. F. Zhou, F. Wang, Y. M. Zhu, Z. P. Liu, *J. Mater. Chem.* **2011**, *21*, 3353.
[11] Y. M. Li, X. J. Lv, J. Lu, J. H. Li, *J. Phys. Chem. C* **2010**, *114*, 21770.
[12] W. C. Ren, Z. S. Wu, L. Wen, L. B. Gao, J. P. Zhao, Z. P. Chen, G. M. Zhou, F. Li, H. M. Cheng, *ACS Nano* **2010**, *4*, 3187.
[13] H. Wang, L. F. Cui, Y. Yang, H. Sanchez Casalongue, J. T. Robinson, Y. Liang, Y. Cui, H. Dai, *J. Am. Chem. Soc.* **2010**, *132*, 13978.
[14] F. Li, G. M. Zhou, D. W. Wang, L. L. Zhang, N. Li, Z. S. Wu, L. Wen, G. Q. Lu, H. M. Cheng, *Chem. Mater.* **2010**, *22*, 5306.
[15] Z. F. Du, X. M. Yin, M. Zhang, Q. Y. Hao, Y. G. Wang, T. H. Wang, *Mater. Lett.* **2010**, *64*, 2076.
[16] D. Li, M. B. Muller, S. Gilje, R. B. Kaner, G. G. Wallace, *Nat. Nanotechnol.* **2008**, *3*, 101.
[17] Y. J. Lee, H. Yi, W. J. Kim, K. Kang, D. S. Yun, M. S. Strano, G. Ceder, A. M. Belcher, *Science* **2009**, *324*, 1051.
[18] X. Dang, H. Yi, M. H. Ham, J. Qi, D. S. Yun, R. Ladewski, M. S. Strano, P. T. Hammond, A. M. Belcher, *Nat. Nanotechnol.* **2011**.
[19] C. F. Barbass III, D. R. Burton, J. K. Scott, G. J. Silverman, *Phage display: a laboratory manual*, Cold Spring Harbor Laboratory Press, New York **2001**.
[20] C. B. Mao, D. J. Solis, B. D. Reiss, S. T. Kottmann, R. Y. Sweeney, A. Hayhurst, G. Georgiou, B. Iverson, A. M. Belcher, *Science* **2004**, *303*, 213.
[21] Y. J. Lee, Y. Lee, D. Oh, T. Chen, G. Ceder, A. M. Belcher, *Nano Lett.* **2010**, *10*, 2433.
[22] T. P. Hopp, K. R. Woods, *Proc. Natl. Acad. Sci. USA Biol. Sci.* **1981**, *78*, 3824.
[23] S. Kneissel, I. Queitsch, G. Petersen, O. Behrsing, B. Micheel, S. Dubel, *J. Mol. Biol.* **1999**, *288*, 21.
[24] M. Bervas, L. C. Klein, G. G. Amatucci, *J. Electrochem. Soc.* **2006**, *153*, A159.
[25] T. A. Albrecht, F. Sauvage, V. Bodenez, J. M. Tarascon, K. R. Poeppelmeier, *Chem. Mater.* **2009**, *21*, 3017.
[26] M. Bervas, B. Yakshinskiy, L. C. Klein, G. G. Amatucci, *J. Am. Ceram. Soc.* **2006**, *89*, 645.
[27] A. J. Gmitter, F. Badway, S. Rangan, R. A. Bartynski, A. Halajko, N. Pereira, G. G. Amatucci, *J. Mater. Chem.* **2010**, *20*, 4149.
[28] B. J. Landi, M. J. Ganter, C. D. Cress, R. A. DiLeo, R. P. Raffaelle, *Energy Environ. Sci.* **2009**, *2*, 638.

Received: September 28, 2011
Published online: February 16, 2012

  